J. Fluid Mech. (1995), *vol.* 302, *pp.* 307–331

Weakly nonlinear analysis of convection in mushy layers during the solidification of binary alloys

By D. M. ANDERSON † AND M. GRAE WORSTER

Institute of Theoretical Geophysics, Department of Applied Mathematics and Theoretical Physics, University of Cambridge, Silver Street, Cambridge CB3 9EW, UK

(Received February 1995)

We consider the solidification of a binary alloy in a mushy layer and analyse the system near the onset of buoyancy-driven convection in the layer. We employ a near-eutectic approximation and consider the limit of large far-field temperature. These asymptotic limits allow us to examine the rich dynamics of the mushy layer in the form of small deviations from the classical case of convection in a horizontal porous layer of uniform permeability. Of particular interest are the effects of the asymmetries in the basic state and the non-uniform permeability in the mushy layer, which lead to transcritically bifurcating convection with hexagonal planform. We obtain a set of three coupled amplitude equations describing the evolution of small-amplitude convecting states in the mushy layer. These equations are analysed to determine the stability of and competition between two-dimensional roll and hexagonal convection patterns. We find that either rolls or hexagons can be stable. Furthermore, hexagons with either upflow or downflow at the centres can be stable, depending on the relative strengths of different physical mechanisms. We determine how to adjust the control parameters to minimize the degree of subcriticality of the bifurcation and hence render the system globally more stable. Finally, the amplitude equations reveal the presence of a new oscillatory instability.

1. Introduction

When a binary mixture is solidified from a cold boundary, the solidification front often becomes morphologically unstable owing to constitutional undercooling (see Kurz & Fisher 1989). The result is a mushy layer, separating the liquid and solid phases, which is a porous medium whose internal structure is composed of fine-scale crystals, through which the residual melt can flow. Buoyancy-driven convection can occur in a mushy layer cooled from below when unstable density gradients are formed as a result of rejection of the lighter component of the mixture upon solidification. Fundamental to the dynamics of the mushy layer is the interaction between convection and solidification.

Compositional convection in the mushy layer has been identified as a means by which non-uniformities in the solid, such as freckles, can be formed. In unidirectionally solidified materials these freckles are vertical channels of different composition

† Present address: Applied and Computational Mathematics Division, National Institute of Standards and Technology, Gaithersburg, MD 20899, USA.

(typically nearer eutectic composition) to the surrounding solid and are appropriately named by their appearance in horizontally cross-sectioned layers of the solid. Freckles have been observed in the casting of metallic alloys and, by comparison with freckles formed in aqueous solutions such as ammonium chloride, have been inferred to be a result of convection through chimneys in the mushy layer (Copley *et al.* 1970; Sample & Hellawell 1984; Sarazin & Hellawell 1988). Freckles are highly undesirable features since they can alter the material and mechanical properties of the solidified alloy. Consequently, there is considerable interest in identifying ways in which to avoid them in practice.

Many laboratory experiments investigating convection in a mushy layer have used aqueous solutions such as ammonium chloride (e.g. Chen & Chen 1991; Tait & Jaupart 1992) because their behaviour during solidification mimics that of their metallic counterparts. Moreover, they are easily handled in the laboratory and their transparent nature allows for the direct visual observation of the solidification process. In such experiments, typically two modes of convection are observed. First, double-diffusive fingers rising from the mush–liquid interface are observed and, later, isolated plumes arising from chimneys in the mushy layer.

A number of theoretical investigations have complemented the experimental studies. Fowler (1985) proposed a model for a mushy layer and analysed a limiting case in which the mushy layer was a non-reacting porous layer and so no coupling between convection and solidification was included in the analysis. Worster (1992*b*) analysed the linear stability of convection in a mushy layer in which he included the effects of the interaction of convection and solidification in the mushy layer. He identified two modes of convective instability corresponding to the two types of convection observed in experiments (e.g. Chen & Chen 1991; Tait & Jaupart 1992). One is a boundary-layer mode, where the convection is driven from a narrow compositional boundary layer above the mush–liquid interface and the mushy layer is relatively undisturbed. The other is a mushy-layer mode in which the convection is driven from the interior of the mushy layer. This mushy-layer mode causes perturbations to the solid fraction, suggesting that this is the mode responsible for the development of chimneys in the mushy layer.

Emms & Fowler (1994) performed a linear stability analysis which involved a time-dependent basic state. In contrast to Worster's (1992*b*) analysis which determined stability relative to a motionless basic state, the linear stability of the mushy-layer convection was determined relative to a basic state that included the effects of double-diffusive, finger-type convection in the liquid. However, the influence of the convection in the liquid upon the mushy layer was found to be negligible in their analysis, indicating that the onset of convection in the mushy layer is little affected by vigorous convection in the melt.

Tait, Jahrling & Jaupart (1992) performed experiments on an ammonium chloride solution in a square tank and, by cooling the base slowly, were able to investigate the planform of chimney convection near onset of convection. Their experiments showed that finger convection in the liquid was observed first with no observable effect on the mushy layer. Later, regions of upflow through the mushy layer and reduced solid fraction formed along the edges of a roughly hexagonal pattern. As these patterns evolved, the upflow occurred mainly at the nodes of the hexagons while that along the edges between the nodes closed off. This hexagonal planform of chimney convection with upflow at the edges and downflow at the centres was observed to be a robust feature of the experiments. The hexagonal pattern of convection observed in the mushy layer is characteristic of near-critical convection and, together with the noted

weak effect of finger convection on the mushy layer, is a signal that there is an internal mechanism controlling the mushy-layer mode.

Linear stability analyses identify the conditions under which the basic state becomes unstable to infinitesimal perturbations. However, it has been suspected (e.g. Fowler 1985; Worster 1992*b*) and recently confirmed (Amberg & Homsy 1993, see below) that the bifurcation to convection in the mushy layer is subcritical. Furthermore, important interactions such as those between perturbations to the solid fraction, and hence the permeability, of the mushy layer and convection are necessarily nonlinear. Therefore, to investigate these issues one must analyse the nonlinear system.

Amberg & Homsy (1993) introduced a model in which the mushy layer was effectively decoupled from the overlying liquid layer and the underlying solid layer. They considered a limit in which the leading-order representation of the mushy layer was that of a non-reacting porous medium of uniform permeability, similar to that of Fowler (1985). However, they then re-introduced effects such as permeability variations as perturbations and thus retained some of the key physical properties of the mushy layer. They performed a weakly nonlinear analysis and identified steady convecting states for both two-dimensional roll and hexagonal planforms. Their results confirmed the presence of subcritical bifurcation for convection in the mushy layer. They found that the bifurcation to rolls could be either supercritical or subcritical and that the bifurcation to hexagonal convection was transcritical. Furthermore, by focusing on the mushy-layer mode of convection they were able to reveal the structure of the mushy-layer convection and its association with flow focusing and remelting.

An issue raised in the results of Amberg & Homsy (1993) was the speculation that hexagons with upflow at the centres would be stable, in contrast to the downflow observed in the experiments by Tait *et al.* (1992). It is well known that hexagonal convection patterns arise as a result of asymmetries in the system associated with various physical effects. Examples of asymmetric (or non-Boussinesq) effects studied in the context of convection are temperature-dependent viscosity (Palm 1960), temperature-dependent material properties such as thermal conductivity and specific heat (Busse 1967), time-dependent boundary conditions such as changing mean temperature (Krishnamurti 1968; Segel 1969), time-periodic heating (Roppo, Davis & Rosenblat 1984), temperature-dependent surface tension (Scanlon & Segel 1967), free-surface deflection (Davis & Segel 1968), and the presence of a solidifying boundary (Davis, Müller & Dietsche 1984; Karcher & Müller 1995). The asymmetry in the analysis of Amberg & Homsy responsible for hexagonal convection was that due to nonlinear perturbations to the permeability of the mushy layer. Here we include other asymmetries associated with the physical effects of curvature in the basic-state density field, higher-order permeability variations, and interactions between the temperature and solid fraction, and by doing so, identify a means by which stable hexagons with upflow at the cell boundaries can be found.

In the present paper, we extend the model of Amberg & Homsy (1993) to study the nonlinear development of the mushy-layer convection further. In particular, we address the question of stability of the finite-amplitude convecting states, including the relative stability between the two-dimensional roll and hexagonal convection. We wish to identify how the subcritical bifurcation, and therefore the global stability limit, varies with the system parameters. We adopt a slightly modified scaling from that of Amberg & Homsy which brings to light a number of new and unexpected features of the system associated with the interactions of heat transfer, convection and solidification in the mushy layer.

Perhaps most surprising of all, we identify the presence of an oscillatory bifurcation which appears to be distinct from the oscillatory mode observed in Chen, Lu & Yang (1994). Those authors extended Worster's (1992*b*) stability analysis and found that when stabilizing thermal buoyancy was present in the liquid the two steady modes of convection could separate by way of an oscillatory connection. They associated this oscillatory mode with the interaction between the double-diffusive convection in the liquid region and the mushy-layer mode of convection. Here, in contrast, there is no region with a statically stable density gradient. We shall discuss the new oscillatory mode identified here only briefly but we analyse it in greater detail in a companion paper (Anderson & Worster 1995).

In §2 we describe the mushy-layer system and formulate the simplified mushy-layer model. In §3 we perform a weakly nonlinear stability analysis and obtain amplitude equations which describe small-amplitude convecting states. In §4 we analyse the amplitude equations and describe the predictions in terms of convection patterns and global (nonlinear) stability boundaries. Finally, in §5, we give the conclusions.

2. Formulation

The physical system we are interested in here is one in which a binary alloy is cooled from below and solidifies releasing a buoyant residual. For mathematical ease we consider a system solidifying at a prescribed constant speed V. This would be the case during the directional casting of turbine blades, for example. In this case, a mushy layer is sandwiched between a completely solid region below (at temperatures below the eutectic) and a completely liquid region above as shown in figure 1. The liquid far above the mushy layer has a composition $C_0 > C_E$ and temperature $T_\infty > T_L(C_0)$ where C_E is the eutectic composition and $T_L(C)$ is the liquidus temperature of the alloy. The model is simplified (Amberg & Homsy 1993) by assuming that the mushy layer is physically isolated, and hence dynamically decoupled, from the overlying liquid and underlying solid regions. This is accomplished by imposing impermeable, rigid, isothermal boundaries at the top and bottom of the mushy layer in a frame of reference moving with the mushy layer at the solidification speed V. These are simplifying assumptions which make the problem analytically tractable but which do not take away the essential physics in the mushy layer associated with interactions between heat transfer, convection and solidification.

The mushy layer is assumed to be in thermodynamic equilibrium so that the temperature T is related to the composition C via the linear liquidus relation

$$T = T_L(C_0) + \Gamma(C - C_0), \tag{2.1}$$

where Γ is the slope of the liquidus. As a result of this direct coupling between temperature and composition, there are no double-diffusive effects within the mushy layer. The liquid density is linearly related to the temperature and composition and from equation (2.1) can be written as

$$\rho_l = \rho_0\left[1 + \beta(C - C_0)\right], \tag{2.2}$$

where $\beta = \beta^* - \Gamma\alpha^*$ and α^* and β^* are the thermal and compositional expansion coefficients, respectively.

It is worth noting that we expect to observe compositional convection as a result of an overall unstable density gradient in the mushy layer. The following physical argument has been put forward as a mechanism by which compositional convection can form chimneys in the mushy layer (e.g. Fowler 1985; Worster 1991; Tait & Jaupart

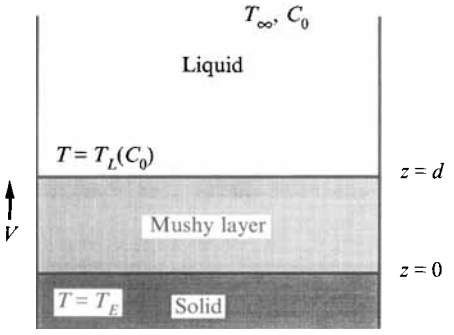

FIGURE 1. The mushy layer system. A binary alloy is cooled from below and releases a buoyant residual upon solidification. The mushy layer is sandwiched between a solid layer (of temperature below the eutectic temperature T_E) and a liquid layer (of temperature above the liquidus temperature $T_L(C_0)$). The liquid far above the mushy layer has a composition C_0 and a temperature $T_\infty > T_L(C_0)$. The mushy layer is assumed to grow upwards into the liquid at a constant speed V and is assumed to have constant thickness d. Conditions corresponding to impermeable, rigid and isothermal boundaries are imposed on the top and bottom of the mushy layer as a simplifying step which effectively decouples the dynamics of the mushy layer from the rest of the system.

1992). When a fluid parcel is displaced upwards in the mushy layer, it finds itself relatively depleted of solute and colder than its surroundings. The fluid parcel, which is assumed to encompass a large number of crystals, reaches thermal equilibrium much more quickly than it can adjust to its new chemical environment owing to the relatively large thermal diffusivity compared with the solute diffusivity. As a result, to maintain thermodynamic equilibrium (as required by the phase diagram) the parcel must dissolve some of the surrounding crystals. This in turn leads to less flow resistance and hence a positive feedback mechanism for the formation of chimneys. This mechanism points towards important interactions between heat transfer, convection and solidification in the mushy layer which we shall address in this paper.

We have used the following scalings to render the governing equations dimensionless. The velocity scale is V, the length and time scales are given by the thermal diffusion length and time, κ/V and κ/V^2, where κ is the thermal diffusivity. The pressure scale is $\kappa\mu/\Pi(0)$ where μ is the viscosity and $\Pi(0)$ is a measure of the permeability of the mushy layer as described below in equation (2.6). The nondimensional temperature (or equivalently composition) is given by

$$\theta = \frac{T - T_L(C_0)}{\Delta T} = \frac{C - C_0}{\Delta C}, \tag{2.3}$$

where $\Delta T = T_L(C_0) - T_E$ and $\Delta C = C_0 - C_E$ so $\Delta T = \Gamma \Delta C$.

The nondimensional equations governing the mushy layer in a reference frame moving at speed V are the heat balance, solute balance, Darcy's equation, and mass balance given by

$$\left(\frac{\partial}{\partial t} - \frac{\partial}{\partial z}\right)(\theta - S\phi) + \boldsymbol{u}\cdot\nabla\theta = \nabla^2\theta, \tag{2.4a}$$

$$\left(\frac{\partial}{\partial t} - \frac{\partial}{\partial z}\right)\left((1-\phi)\theta + \mathscr{C}\phi\right) + \boldsymbol{u}\cdot\nabla\theta = 0, \tag{2.4b}$$

$$K(\phi)\boldsymbol{u} = -\nabla p - Ra\theta\hat{\boldsymbol{z}}, \tag{2.4c}$$

$$\nabla\cdot\boldsymbol{u} = 0. \tag{2.4d}$$

The basis for these equations rests on the idea that, owing to its fine-scale structure, the mushy layer can be treated as a continuum. The derivation and justification of equations such as these as continuum descriptions of the mushy layer have been put forward by a number of previous authors (e.g. Hills, Loper & Roberts 1983; Worster 1986; Bennon & Incropera 1987; Voller & Brent 1989; Worster 1992*a*). The present formulation and notation is most similar to that of Worster (1992*b*), which was also used by Amberg & Homsy (1993). We have taken the material properties of the solid and liquid phases to be equal and have neglected diffusion of solute. Note, however, that since the mushy layer is in thermodynamic equilibrium, retaining the effect of solute diffusion here would effectively only modify the coefficient of the diffusion term in equation (2.4*a*) but slightly. The dimensionless parameters appearing in these equations are the Stefan number S, the concentration ratio $\mathscr{C}$, and the Rayleigh number Ra, where

$$S = \frac{L}{c_l \Delta T}, \tag{2.5a}$$

$$\mathscr{C} = \frac{C_S - C_0}{C_0 - C_E}, \tag{2.5b}$$

$$Ra = \frac{\beta \Delta C g \Pi(0) \kappa / V}{\nu \kappa}, \tag{2.5c}$$

where L is the latent heat, c_l is the specific heat, C_S is the solid composition, C_E is the eutectic composition, g is gravity, and ν is the kinematic viscosity of the liquid. The Stefan number S gives a measure of the latent heat relative to the heat content, or available heat in the system. The compositional ratio $\mathscr{C}$ relates the difference in characteristic compositions of the liquid and solid phases with the compositional variation of the liquid within the mushy layer. Large values of $\mathscr{C}$, which we shall consider shortly, correspond to initial compositions which are near the eutectic composition. The Rayleigh number Ra measures the destabilizing influence of compositional buoyancy relative to the stabilizing influence of thermal diffusion.

The function $K(\phi)$ measures the variation of the permeability $\Pi(\phi)$ with local solid fraction ϕ and is given by

$$K(\phi) = \frac{\Pi(0)}{\Pi(\phi)}, \tag{2.6}$$

where the permeability is assumed to be finite for zero solid fraction. Such an assumption, as discussed by Worster (1992*b*), is appropriate when Darcy's equation, rather than a more general Brinkman equation, which includes the effects of inertia and deviatoric stresses in the mushy layer, is used to describe the flow.

Equations (2.4) are subject to the imposed boundary conditions

$$\theta = -1, \; w = 0 \quad \text{at} \quad z = 0, \tag{2.7a,b}$$

$$\theta = 0, \; w = 0, \; \phi = 0 \quad \text{at} \quad z = \delta, \tag{2.8a–c}$$

where $\delta = d/(\kappa/V)$ is the dimensionless depth of the layer. The solid–mush interface $z = 0$ is at the eutectic temperature and is impermeable. The mush–liquid interface $z = \delta$ is at the liquidus temperature, is impermeable, and corresponds to zero solid fraction.

The hydrodynamic boundary condition for the fully dynamic two-layer problem where the mushy layer and liquid layer are coupled is one of continuity of pressure $[p] = 0$ at the mush–liquid interface. This condition reduces to that of p =constant

on the mush–liquid interface in the limit of zero Darcy number $Da = \Pi(0)/(\kappa/V)^2$, where the Darcy number measures the ratio of the average spacing between the crystals in the mushy layer to the thermal length (Emms & Fowler 1994). Here we are imposing artificially the no-flow condition (2.8*b*) instead of the pressure condition and we are additionally keeping the position of the interface $z = \delta$ fixed. These approximations, which were introduced by Amberg & Homsy, render the nonlinear analysis analytically tractable. With the exception of (2.8*b*) these boundary conditions are those for the full system in the limit of infinite Lewis number (the ratio of thermal to solutal diffusivities in the liquid) though in that case δ is a variable determined by continuity of heat flux at the mush–liquid interface. These simplifying assumptions should not jeopardize our ability to capture essential interactions between heat transfer, convection and solidification in the mushy layer.

We can associate the dimensionless mushy-layer thickness δ with the inverse of the nondimensional far-field temperature $\theta_\infty = (T_\infty - T_L(C_0))/\Delta T$ by noting that when a liquid layer is present above the mushy layer, equating the temperature gradient in the mushy layer $\Delta T/d$ with the temperature gradient in the liquid $(T_\infty - T_L(C_0))/(\kappa/V)$ gives $\delta \sim 1/\theta_\infty$. Furthermore, Worster (1991) showed, by analysing the exact solution for a non-convecting mushy layer, that as $\theta_\infty \to \infty$ the mushy-layer thickness is given by

$$\delta \sim \ln\left(1 + \frac{1}{\theta_\infty}\right) \sim \frac{1}{\theta_\infty} + \ldots \tag{2.9}$$

(see also Fowler 1985).

We follow Amberg & Homsy (1993) in rescaling the model which corresponds to a thin mushy layer in the limit $\delta \ll 1$. We consider the limit where $\mathscr{C}$ is large. Physically, this corresponds to the case where the initial composition of the liquid is close to the eutectic composition as can be seen by the definition of $\mathscr{C}$ in equation (2.5*b*). Specifically, we take

$$\mathscr{C} = \frac{C_S}{\delta}, \tag{2.10}$$

where C_S is $O(1)$ as $\delta \to 0$. The above approximation ($\delta \to 0$, $\mathscr{C} \to \infty$) corresponds to the near-eutectic approximation used by Fowler (1985).

We shall see that the main effect of large $\mathscr{C}$ is to give small solid fraction, and hence nearly uniform permeability, and the main effect of small δ is to give a nearly linear basic-state density profile. Therefore, this limit allows for the leading-order description of the mushy layer as a porous layer of constant permeability subject to a linear density gradient. The idea is then to re-introduce effects such as permeability variations and nonlinear density gradients as perturbations to this simpler system. Note that experiments with ammonium chloride have had large values of $\mathscr{C}$ (typically $\mathscr{C} \approx 20$) so that the mushy layers in the experiments have had small solid fraction and nearly uniform permeability. The value of δ has not been particularly small in experiments conducted to date. However, we explore the effects of nonlinear density gradients by allowing perturbations in δ to the near-eutectic approximation. In contrast to Amberg & Homsy (1993) who kept $S = O(1)$, we follow Emms & Fowler (1994) and assume that the Stefan number is large by writing

$$S = \frac{\bar{S}}{\delta}, \tag{2.11}$$

where $\bar{S}$ is $O(1)$ as $\delta \to 0$. We shall find that this leads to a number of interesting

results. Also, the results derived with S scaled in this way can readily be reduced to the case studied by Amberg & Homsy (1993), and we shall recover results for that case. Following Amberg & Homsy we rescale space and time and also introduce a new effective Rayleigh number R based on the mushy-layer thickness δ

$$(x, y, z) = \delta(\bar{x}, \bar{y}, \bar{z}), \tag{2.12a}$$

$$t = \delta^2 \bar{t}, \tag{2.12b}$$

$$R^2 = \delta Ra. \tag{2.12c}$$

We seek solutions to the system (2.4) by perturbing about a motionless basic state, in the moving frame, where the temperature θ_B and solid fraction ϕ_B vary only in the vertical direction. The small perturbations are measured by a perturbation amplitude ϵ and can vary horizontally, vertically and temporally. Specifically, we take

$$\theta = \theta_B(\bar{z}) + \epsilon\hat{\theta}(\bar{x}, \bar{y}, \bar{z}, \bar{t}), \tag{2.13a}$$

$$\phi = \phi_B(\bar{z}) + \epsilon\hat{\phi}(\bar{x}, \bar{y}, \bar{z}, \bar{t}), \tag{2.13b}$$

$$\boldsymbol{u} = 0 + \epsilon\frac{R}{\delta}\hat{\boldsymbol{u}}(\bar{x}, \bar{y}, \bar{z}, \bar{t}), \tag{2.13c}$$

$$p = Rp_B(\bar{z}) + R\epsilon\hat{p}(\bar{x}, \bar{y}, \bar{z}, \bar{t}), \tag{2.13d}$$

where we assume that $\epsilon \ll \delta \ll 1$ (further discussion of this is given in §3).

The steady basic state, denoted by subscript 'B', is horizontally uniform and satisfies

$$-\delta\frac{\mathrm{d}}{\mathrm{d}\bar{z}}\left(\theta_B - \frac{\bar{S}}{\delta}\phi_B\right) = \frac{\mathrm{d}^2\theta_B}{\mathrm{d}\bar{z}^2}, \tag{2.14a}$$

$$-\delta\frac{\mathrm{d}}{\mathrm{d}\bar{z}}\left((1-\phi_B)\theta_B + \frac{C_S}{\delta}\phi_B\right) = 0, \tag{2.14b}$$

$$-\frac{\mathrm{d}p_B}{\mathrm{d}\bar{z}} - R\theta_B = 0, \tag{2.14c}$$

subject to the boundary conditions

$$\theta_B = -1 \quad \text{at} \quad \bar{z} = 0, \tag{2.15}$$

$$\theta_B = 0, \ \phi_B = 0 \quad \text{at} \quad \bar{z} = 1. \tag{2.16a,b}$$

We can express the basic-state solutions in terms of asymptotic expansions for $\delta \ll 1$,

$$\theta_B = (\bar{z} - 1) - \delta\frac{\Omega}{2}(\bar{z}^2 - \bar{z}) + \ldots, \tag{2.17a}$$

$$\phi_B = \delta\bar{\phi}_B = -\delta\frac{\bar{z} - 1}{C_S} + \delta^2\left(-\frac{(\bar{z}-1)^2}{C_S^2} + \frac{\Omega}{2C_S}(\bar{z}^2 - \bar{z})\right) + \ldots, \tag{2.17b}$$

where $\Omega = 1 + \bar{S}/C_S$. Note that the assumption that $\mathscr{C} \sim O(1/\delta)$ leads to small basic-state solid fraction of $O(\delta)$. In the limit $\delta \to 0$ we find that the system corresponds to convection in a passive porous medium with a linear temperature gradient as considered by Palm, Weber & Kvernvold (1972). Effects which are fundamental to the mushy layer are re-introduced as small perturbations (in δ) to this simpler system. Note also that, with the rescaling of the Stefan number, the basic state is slightly modified from that of Amberg & Homsy.

The perturbation equations are

$$\left(\frac{\partial}{\partial \bar{t}} - \delta\frac{\partial}{\partial \bar{z}}\right)\left(\hat{\theta} - \frac{\bar{S}}{\delta}\hat{\phi}\right) + R\hat{w}\frac{\mathrm{d}\theta_B}{\mathrm{d}\bar{z}} - \nabla^2\hat{\theta} = -\epsilon R\hat{\boldsymbol{u}}\cdot\nabla\hat{\theta}, \quad (2.18a)$$

$$\left(\frac{\partial}{\partial \bar{t}} - \delta\frac{\partial}{\partial \bar{z}}\right)\left((1-\delta\bar{\phi}_B)\hat{\theta} - \theta_B\hat{\phi} - \epsilon\hat{\phi}\hat{\theta} + \frac{C_S}{\delta}\hat{\phi}\right) + R\hat{w}\frac{\mathrm{d}\theta_B}{\mathrm{d}\bar{z}} = -\epsilon R\hat{\boldsymbol{u}}\cdot\nabla\hat{\theta}, \quad (2.18b)$$

$$\nabla^2\left[K(\delta\bar{\phi}_B + \epsilon\hat{\phi})\hat{w}\right] - \frac{\partial}{\partial\bar{z}}\left[\hat{\boldsymbol{u}}\cdot\nabla K(\delta\bar{\phi}_B + \epsilon\hat{\phi})\right] + R\nabla_2^2\hat{\theta} = 0, \quad (2.18c)$$

$$\nabla^2\left[K(\delta\bar{\phi}_B + \epsilon\hat{\phi})\hat{u}\right] - \frac{\partial}{\partial\bar{x}}\left[\hat{\boldsymbol{u}}\cdot\nabla K(\delta\bar{\phi}_B + \epsilon\hat{\phi})\right] - R\frac{\partial^2\hat{\theta}}{\partial\bar{x}\partial\bar{z}} = 0, \quad (2.18d)$$

$$\nabla^2\left[K(\delta\bar{\phi}_B + \epsilon\hat{\phi})\hat{v}\right] - \frac{\partial}{\partial\bar{y}}\left[\hat{\boldsymbol{u}}\cdot\nabla K(\delta\bar{\phi}_B + \epsilon\hat{\phi})\right] - R\frac{\partial^2\hat{\theta}}{\partial\bar{y}\partial\bar{z}} = 0, \quad (2.18e)$$

$$\nabla\cdot\hat{\boldsymbol{u}} = 0, \quad (2.18f)$$

subject to the boundary conditions

$$\hat{\theta} = 0,\ \hat{w} = 0 \quad \text{at} \quad \bar{z} = 0, \quad (2.19a,b)$$

$$\hat{\theta} = 0,\ \hat{w} = 0,\ \hat{\phi} = 0 \quad \text{at} \quad \bar{z} = 1. \quad (2.20a\text{–}c)$$

Since the basic-state solid fraction is small and the perturbations to the solid fraction will also be small, we follow Amberg & Homsy and expand the function $K(\phi)$ in a Taylor series for $\phi \ll 1$

$$K(\phi) = 1 + K_1\phi + K_2\phi^2 + K_3\phi^3 + \ldots. \quad (2.21)$$

The specific form of the permeability as a function of the local solid fraction is then characterized by the coefficients $K_1, K_2, K_3, \ldots$. We shall not specify a particular form for the permeability now but we shall require that $K_1 > 0$ so that the permeability decreases with increasing solid fraction. Later, we shall focus on a particular limiting case where K_1 is 'small', formally of the same order as the dimensionless mushy-layer thickness δ.

3. Weakly nonlinear analysis

We follow a standard weakly nonlinear approach (e.g. Busse 1967) in describing the onset of convection in the mushy layer. Here we have two small parameters, the mushy-layer thickness δ and the perturbation amplitude ϵ. We consider the formal asymptotic expansions in the *double* limit $\lim_{\delta\to 0}[\lim_{\epsilon\to 0} f(\delta,\epsilon)]$ of functions $f(\delta,\epsilon)$. In other words, we consider $\delta = O(1)$ as $\epsilon \to 0$. The procedure is first to make a formal asymptotic expansion in $\epsilon \ll 1$ and then at each order in ϵ make a formal asymptotic expansion in $\delta \ll 1$. Note that this is quite different from the limit $\lim_{\epsilon\to 0}[\lim_{\delta\to 0} f(\delta,\epsilon)]$. Indeed, as we shall see, the system is singular in the limit $\delta \to 0$ with $\epsilon = O(1)$. Our approach is also different from that used by Amberg & Homsy (1993) who took the *distinguished* limit $\delta = O(\epsilon)$ as $\epsilon \to 0$. Their results are recoverable from ours by setting $\delta = \epsilon$, as we shall show later.

The different scaling of the Stefan number S in our analysis as compared with Amberg & Homsy (1993) changes the basic state as well as the perturbation equations. However, we find that by introducing the following additional scalings on $\hat{\phi}$, $\hat{\boldsymbol{u}}$ and R involving the $O(1)$ parameter $\Omega = 1 + S/\mathscr{C}$, the leading-order perturbation equations

are identical to theirs. The expansions for the perturbation quantities are

$$\hat{\theta} = (\theta_{00} + \delta\theta_{01} + \ldots) + \epsilon(\theta_{10} + \delta\theta_{11} + \ldots) + \epsilon^2(\theta_{20} + \delta\theta_{21} + \ldots) + \ldots, \tag{3.1a}$$

$$\Omega\hat{\phi} = (\phi_{00} + \delta\phi_{01} + \ldots) + \epsilon(\phi_{10} + \delta\phi_{11} + \ldots) + \epsilon^2(\frac{1}{\delta}\phi_{2(-1)} + \phi_{20} + \delta\phi_{21} + \ldots) + \ldots, \tag{3.1b}$$

$$\Omega^{1/2}\hat{\boldsymbol{u}} = (\hat{\boldsymbol{u}}_{00} + \delta\hat{\boldsymbol{u}}_{01} + \ldots) + \epsilon(\hat{\boldsymbol{u}}_{10} + \delta\hat{\boldsymbol{u}}_{11} + \ldots) + \epsilon^2(\hat{\boldsymbol{u}}_{20} + \delta\hat{\boldsymbol{u}}_{21} + \ldots) + \ldots, \tag{3.1c}$$

$$\Omega^{1/2}R = (R_{00} + \delta R_{01} + \ldots) + \epsilon(R_{10} + \delta R_{11} + \ldots) + \epsilon^2(R_{20} + \delta R_{21} + \ldots) + \ldots. \tag{3.1d}$$

Note that the expansion of $\hat{\phi}$ is singular at $O(\epsilon^2)$ as $\delta \to 0$. Therefore, if a distinguished limit of the equations is sought, rather than the double limit considered here, then it is essential to insist that $\epsilon^2 \ll \delta$. The distinguished limit $\delta = O(\epsilon)$ considered by Amberg & Homsy (1993) satisfies this constraint and is therefore consistent with our approach. We find that the correct treatment of this term leads to an important interaction between convection and solidification in the mushy layer that results in an oscillatory instability. We discuss this term further below.

The leading-order solutions ($O(\epsilon^0\delta^0)$) to the perturbation equations (2.18) are

$$\theta_{00} = -\sin(\pi\bar{z})\,\eta(\bar{x},\bar{y}), \tag{3.2a}$$

$$\phi_{00} = -\frac{2\pi}{C_S}(\cos(\pi\bar{z}) + 1)\,\eta(\bar{x},\bar{y}), \tag{3.2b}$$

$$w_{00} = \pi\sin(\pi\bar{z})\,\eta(\bar{x},\bar{y}), \tag{3.2c}$$

$$u_{00} = \cos(\pi\bar{z})\,\frac{\partial\eta(\bar{x},\bar{y})}{\partial\bar{x}}, \tag{3.2d}$$

$$v_{00} = \cos(\pi\bar{z})\,\frac{\partial\eta(\bar{x},\bar{y})}{\partial\bar{y}}, \tag{3.2e}$$

$$R_{00} = 2\pi, \tag{3.2f}$$

where the two-dimensional planform which describes rolls and hexagons is

$$\eta(\bar{x},\bar{y}) = \sum_{j=1}^{3}\left(A_j(\tau)\mathrm{e}^{\mathrm{i}\boldsymbol{a}_j\cdot\boldsymbol{r}} + A_j^*(\tau)\mathrm{e}^{-\mathrm{i}\boldsymbol{a}_j\cdot\boldsymbol{r}}\right), \tag{3.3}$$

with

$$\boldsymbol{a}_j = \{(0,\pi),(\frac{\sqrt{3}\pi}{2},\frac{\pi}{2}),(\frac{\sqrt{3}\pi}{2},-\frac{\pi}{2})\}\ ,\ \boldsymbol{r} = (\bar{x},\bar{y}), \tag{3.4}$$

and τ is a slow time scale defined below. When $A_1 = A_2 = A_3 \neq 0$ the pattern corresponds to hexagons and when $A_i \neq 0$ and $A_j = 0$ for $j \neq i$ the pattern corresponds to two-dimensional rolls. The wavenumber corresponding to the minimum value of the linear, critical Rayleigh number is $k = \pi$ and we fix this value throughout our analysis. The critical Rayleigh number and corresponding wavenumber as well as the two-dimensional version of the thermal and flow fields are identical to those of Palm *et al.* (1972) who considered steady convection in a passive porous medium. When $A_1 = \frac{1}{2}$ and $A_2 = A_3 = 0$ the planform corresponds to the two-dimensional roll solution of Amberg & Homsy (1993) and when $A_1 = A_2 = A_3 = \frac{1}{2}$ the planform corresponds to their hexagonal solution. In their analysis, the solvability conditions required for the existence of higher-order solutions determined R_{10}, R_{11}, etc. and by solving the expansion of R for ϵ they were able to identify steady finite-amplitude solutions. In the present analysis we are interested in the stability of such solutions,

and so the amplitudes $A_j(\tau)$, which are functions of a slow time scale $\tau = \epsilon^2\bar{t}$, are determined via solvability conditions. This scaling for the slow time scale τ is suggested by linear theory and indicates that the nonlinear development of the solution occurs slowly and is consistent with the Rayleigh number being near its critical value corresponding to onset of instability.

At $O(\epsilon^0\delta)$ we obtain the first correction terms in δ. These involve undetermined amplitudes $B_j(\tau)$ through an analogous planform

$$\eta^{(B)}(\bar{x},\bar{y}) = \sum_{j=1}^{3}\left(B_j(\tau)e^{i\boldsymbol{a}_j\cdot\boldsymbol{r}} + B_j^*(\tau)e^{-i\boldsymbol{a}_j\cdot\boldsymbol{r}}\right). \tag{3.5}$$

So, for example,

$$\theta_{01} = -\sin(\pi\bar{z})\,\eta^{(B)}(\bar{x},\bar{y}) + f_\theta(\bar{z})\eta(\bar{x},\bar{y}), \tag{3.6}$$

where $f_\theta(\bar{z})$ corresponds to the $\bar{z}$-dependence of the particular solution forced at this order. Then

$$\theta_{00} + \delta\theta_{01} = [-\sin(\pi\bar{z}) + \delta f_\theta(\bar{z})]\left[\eta(\bar{x},\bar{y}) + \delta\eta^B(\bar{x},\bar{y})\right] + O(\delta^2), \tag{3.7}$$

where the planform here gives rise to the amplitudes of interest $\mathscr{A}_j \equiv A_j + \delta B_j$. We refrain from showing further solutions at this order except to note that

$$R_{01} = \frac{\bar{S}}{C_S^2\Omega}\left(\frac{4}{\pi} + \frac{\pi}{2}\right). \tag{3.8}$$

The higher-order correction terms in the expansions (3.1) which we calculated symbolically using Mathematica become increasingly tedious and are not presented here. However, there are important steps and assumptions along the way to obtaining amplitude equations which we shall point out.

To understand our approach at this stage of the analysis, it is helpful to consider the results of Amberg & Homsy (1993). They found steady solutions to the weakly nonlinear system in the form of two-dimensional rolls and hexagons. For two-dimensional rolls they found (in their notation) that

$$R = \left(2\pi + \delta R_{1\delta} + \delta^2 R_{2\delta} + \ldots\right) + \epsilon^2 R_{2\epsilon} + \ldots. \tag{3.9}$$

The sign of $R_{2\epsilon}$ determines whether rolls are supercritical or subcritical. They identified a critical value ($K_1/C_S = 0.226$) of the parameter combination K_1/C_S below which the bifurcation to rolls was supercritical and above which the bifurcation was subcritical. For hexagons they found that

$$R = (2\pi + \delta R_{1\delta} + \ldots) + \epsilon R_{1\epsilon} + \ldots, \tag{3.10}$$

so that the bifurcation to hexagons was transcritical. They found that $R_{1\epsilon}$ was proportional to the same parameter combination K_1/C_S. (Note: the value of $R_{1\epsilon}$ was incorrectly given in their paper as $-(\frac{136}{9} + \frac{3}{2}\pi^2)K_1/C_S$. It should be $-\frac{3}{2}\pi^2 K_1/C_S$ (private communication, Amberg 1994).)

In their discussion of these results Amberg & Homsy speculated on the possible interaction between two-dimensional roll and hexagonal convection patterns based on fundamental ideas of bifurcation theory. This led them to the conclusion that their results would predict stable hexagons with upflow in the centres and *unstable* hexagons with downflow at the centres. They pointed out that this prediction conflicted with experimental results of Tait *et al.* (1992) who observed hexagons with downflow at the centres.

It is well known that hexagonal convection patterns arise as a result of various asymmetries in the system. The particular physical effect which gave rise to hexagons in the Amberg & Homsy analysis was that associated with the term K_1/C_S, namely nonlinear permeability variations associated with perturbations to the basic-state solid fraction. Since both K_1 and C_S are always positive, the nature of the transcritical bifurcation based on this result could not vary. However, there are a number of other physical effects in this system which also cause asymmetries but which correspond to higher-order terms that were neglected in the analysis of Amberg & Homsy. That is, for example, they did not calculate $O(\delta)$ corrections for the term $R_{1\epsilon}$.

We extend their analysis in two ways. First, we consider the case where the hexagonal bifurcation is nearly vertical so that both two-dimensional roll and hexagon patterns can be captured local to the bifurcation point in the same stability analysis. This can be accomplished by taking K_1/C_S to be formally of $O(\delta)$ as described below. Secondly, we include additional physical effects that can also lead to hexagonal convection in this system. Since the physical effect identified by Amberg & Homsy appeared as a term proportional to K_1/C_S, the $O(\delta)$ correction terms corresponding to the other physical effects become important when K_1/C_S is also $O(\delta)$. Therefore, the limit where K_1/C_S is small is of dual interest.

To accomplish these goals in our analysis we wish to choose the value of K_1/C_S so that the transcritical bifurcation to hexagons, the nature of which is determined by the combined effect of *a variety of* physical effects, is near the vertical bifurcation. Said another way, we expand K_1 about a critical value, determined by the other physical effects, in such a way that the combination of these effects leads to near vertical bifurcation of the hexagonal branch. In terms of our weakly nonlinear stability analysis we solve the $O(\epsilon)$ problem (correct to $O(\delta)$) and find that the existence of solutions requires that

$$R_{10} = -\frac{3\pi^2}{2}\frac{K_1}{C_S}, \tag{3.11a}$$

$$R_{11} = -\frac{4}{3}\Omega^2 - \left(\frac{44}{9} + \frac{3\pi^2}{2}\right)\frac{K_2}{C_S^2} + \frac{26}{7}\frac{\bar{S}}{C_S^2} + g(K_1). \tag{3.11b}$$

Note that $g(K_1)$ was not calculated explicitly in the present analysis (in anticipation of considering the limit of small K_1) but has the property that $g(0) = 0$. The value of R_{10} corresponds to $R_{1\epsilon}$ in the analysis of hexagons in Amberg & Homsy (1993). New here is the expression for R_{11}, which represents higher-order physical effects as discussed above. Now, in order to capture both two-dimensional rolls and hexagons in the same stability analysis $R_{10} + \delta R_{11}$ must be equal to zero (that is, to this order, the bifurcation to hexagons is vertical). We accomplish this by making the following assumption about K_1. We take

$$K_1 = \delta K_c + \delta\epsilon\bar{K}_1, \tag{3.12}$$

where

$$\frac{K_c}{C_S} = \frac{2}{3\pi^2}\left[-\frac{4}{3}\Omega^2 - \left(\frac{44}{9} + \frac{3\pi^2}{2}\right)\frac{K_2}{C_S^2} + \frac{26}{7}\frac{\bar{S}}{C_S^2}\right], \tag{3.13}$$

and $\bar{K}_1$ measures the variation to either side of this critical value.

Equation (3.13) embodies various physical effects which lead to hexagonal convection. The term K_c/C_S represents nonlinear permeability variations associated with perturbations to the solid fraction. Note that by our choice of K_1 to be $O(\delta)$, varia-

tions in permeability due to variations in the basic-state solid fraction are $O(\delta^2)$ and therefore have not been included in this analysis. Such terms would appear in $g(K_1)$ and become negligible at this order when K_1 is $O(\delta)$. The first term in the square brackets in equation (3.13) is associated with curvature in the temperature profile. This is an effect due to the uniform vertical translation of the mushy layer in time (as viewed in the laboratory frame). The second term in the brackets is associated with higher-order nonuniformity of the permeability due to the basic-state solid fraction and its perturbations. The final term in the brackets represents linear and nonlinear interactions of temperature and solid fraction. We shall discuss these further in §4.

Next, we discuss the appearance of the $O(1/\delta)$ term in the expansion for solid fraction perturbation $\hat{\phi}$ as indicated in equation (3.1*b*). We find that the $O(\epsilon^2)$ problem is forced by a term of $O(1/\delta)$ in the solute balance (2.18*b*). This is the reason for the $O(1/\delta)$ term in the expansion for solid-fraction perturbation $\hat{\phi}$. Specifically we find that at $O(\epsilon^2\delta^{-1})$

$$-C_S\frac{\partial\phi_{2(-1)}}{\partial\bar{z}} = -C_S\frac{\partial\phi_{00}}{\partial\tau}, \tag{3.14}$$

so that $\phi_{2(-1)}$ is directly proportional to a time derivative. In terms of the small amplitude parameter ϵ, the time scale τ measures slow variations in time of $O(\epsilon^2)$ associated with the disturbance growth rate. In terms of the small dimensionless mushy-layer thickness δ, the time scale $\tau = O(\delta^2)$ is characteristic of the diffusion time across the layer. The balance in equation (3.14) suggests that a different time scale, of $O(\delta)$, is appropriate, i.e. the time associated with the mushy-layer thickness and the vertical translation speed of the mushy layer. In what follows, we shall see that this term has a key effect on the dynamics of the mushy layer.

We next define the amplitude $\mathscr{A}_j = A_j + \delta B_j$, where the amplitudes B_j are the analogues of A_j appearing at $O(\delta)$ as described above. The amplitudes $\mathscr{A}_j$ correspond to the $O(\epsilon)$ terms, correct to $O(\delta)$, in the perturbations to the basic-state solutions. We combine the results of the solvability conditions found at $O(\epsilon^3\delta^0)$ and $O(\epsilon^3\delta)$ to obtain the set of coupled evolution equations

$$a\dot{\mathscr{A}}_1 = 2\pi R_2\mathscr{A}_1 + b\mathscr{A}_2\mathscr{A}_3^* - c\mathscr{A}_1|\mathscr{A}_1|^2 - d\mathscr{A}_1(|\mathscr{A}_2|^2 + |\mathscr{A}_3|^2), \tag{3.15a}$$

$$a\dot{\mathscr{A}}_2 = 2\pi R_2\mathscr{A}_2 + b\mathscr{A}_1\mathscr{A}_3 - c\mathscr{A}_2|\mathscr{A}_2|^2 - d\mathscr{A}_2(|\mathscr{A}_1|^2 + |\mathscr{A}_3|^2), \tag{3.15b}$$

$$a\dot{\mathscr{A}}_3 = 2\pi R_2\mathscr{A}_3 + b\mathscr{A}_1^*\mathscr{A}_2 - c\mathscr{A}_3|\mathscr{A}_3|^2 - d\mathscr{A}_3(|\mathscr{A}_1|^2 + |\mathscr{A}_2|^2), \tag{3.15c}$$

where

$$a = \left(\Omega - 2\frac{\bar{S}}{C_S^2\Omega}\right) + \delta a_1, \tag{3.16a}$$

$$b = 6\pi^3\delta\frac{\bar{K}_1}{\Omega C_S}, \tag{3.16b}$$

$$c = 2\pi^4\left(1 + 11\frac{K_2}{\Omega^2 C_S^2}\right) + \delta c_1, \tag{3.16c}$$

$$d = 2\pi^4\left(\frac{410}{259} + 22\frac{K_2}{\Omega^2 C_S^2}\right) + \delta d_1, \tag{3.16d}$$

$$R_2 = R_{20} + \delta R_{21}. \tag{3.16e}$$

Expressions for a_1, c_1 and d_1 are given in the Appendix. Such equations are familiar in convection (e.g. Segel 1965) as well as a variety of other physical systems, such as solidification (Brattkus & Davis 1988) and combustion (Kuske & Matkowsky 1994)

and their solutions are well known. The form of such equations can be predicted on the basis of symmetries and group theoretical arguments (e.g. Golubitsky, Swift & Knobloch 1984). The important result here, and that which largely reflects the computational effort in the analysis, is the calculation of the particular coefficients that appear in these equations.

4. Analysis of amplitude equations

The amplitude equations (3.15) reveal a variety of results regarding convection in the mushy layer. We first note that the coefficient a of the time derivative can vanish. That is, there exist physically allowable parameter values for which a (see equation (3.16a)) can be positive, negative or zero. This suggests the possibility of a Hopf bifurcation. So our analysis of the steady convective instability in the mushy layer has revealed the presence of hitherto unsuspected oscillatory instability. We have subsequently reconsidered the linear stability problem and have indeed found an oscillatory instability. We find that the point at which this coefficient vanishes corresponds to the appearance of the oscillatory mode at the minimum of the neutral stability curve for the real mode. We have found that it is the contribution from the singular term $\phi_{2(-1)}$ in equation (3.1b) which gives rise to this oscillatory instability. We present these calculations in a companion paper (Anderson & Worster 1995). In the analysis which follows we shall treat those cases away from this point (so that $a > 0$) and consider solutions to the evolution equations (3.15) in the form of two-dimensional rolls and hexagons. The parameter regime where these results are appropriate are discussed in more detail below.

4.1. *Convection patterns*

Another new feature of the system is that the coefficient of the quadratic term in (3.15) can be positive or negative. This implies, as we shall see, that hexagons with either upflow in the centre (up hexagons) or downflow in the centre (down hexagons) can be stable. By analysing the hexagonal solution to the amplitude equations (3.15), using equations (3.12), (3.13) and (3.16b) and converting back to original variables we find that the sense of the flow is determined by the sign of

$$\epsilon b = \frac{6\pi^3}{\Omega}\left\{\frac{K_1}{\delta\mathscr{C}} + \frac{2\delta}{3\pi^2}\left[\frac{4}{3}\Omega^2 + \left(\frac{44}{9} + \frac{3\pi^2}{2}\right)\frac{K_2}{\delta^2\mathscr{C}^2} - \frac{26}{7}\frac{S}{\delta\mathscr{C}^2}\right]\right\}, \tag{4.1}$$

with (stable) up hexagons corresponding to $\epsilon b > 0$ and (stable) down hexagons corresponding to $\epsilon b < 0$. Note that by our assumptions (2.10), (2.11) and (3.12), each of the terms on the right-hand side of this expression is $O(\delta)$. These terms represent all the physical effects included in this analysis that lead to hexagonal convection.

Figure 2 shows bifurcation diagrams for solutions of equations (3.15) corresponding to steady finite-amplitude convection in the form of two-dimensional rolls ($\mathscr{A}_1$ = real, $\mathscr{A}_2 = \mathscr{A}_3 = 0$), hexagons ($\mathscr{A}_1 = \mathscr{A}_2 = \mathscr{A}_3 =$ real), and a mixed mode ($\mathscr{A}_1$ = real, $\mathscr{A}_2 = \mathscr{A}_3 =$ real). The solid portions of the curves indicate where the solutions are linearly stable while the dashed portions indicate where the solutions are linearly unstable. We see that the two-dimensional roll solution is supercritical and initially unstable to a subcritically bifurcating hexagonal solution. The mixed-mode solution, which is always unstable, connects the two-dimensional roll solution and the hexagonal solution at the points along those branches where their stability changes. Where the mixed mode attaches to the roll branch, $\mathscr{A}_2 = \mathscr{A}_3 = 0$ and $\mathscr{A}_1 = A^{(r,h)}$. The amplitudes $\mathscr{A}_2 = \mathscr{A}_3$ vary along the mixed-mode branch and $\mathscr{A}_1 = \mathscr{A}_2 = \mathscr{A}_3 = A^{(r,h)}$

at the point where the mixed mode connects with the hexagonal branch. Note that in the analysis of Amberg & Homsy the two-dimensional roll solution was found to be supercritical when $K_1/C_S < 0.226$ and subcritical for $K_1/C_S > 0.226$ (for the case $K_2 = 0$). Here K_1/C_S is $O(\delta)$ and so the bifurcation to rolls is always supercritical. Figure 2(*a*) shows the bifurcation diagram for the case where $\epsilon b > 0$ while figure 2(*b*) shows the case where $\epsilon b < 0$ (see equation (4.1)). The case where $\epsilon b > 0$ was anticipated by Amberg & Homsy and shows that although either two-dimensional roll or hexagonal convection patterns can be stable, only hexagonal convection with *upflow* at the centres (up hexagons) can be stable (see figure 2*a*). However, the present analysis reveals that, with the inclusion of further physical effects in the problem, it is now possible for $\epsilon b < 0$ so that hexagons with downflow at the centre (down hexagons) are stable (see figure 2*b*), as observed in the experiments by Tait *et al.* (1992). It should be noted that it is the existence of *stable* down hexagons which is made possible when $\epsilon b < 0$. When $\epsilon b > 0$ there exist down hexagons for negative amplitudes (see figure 2a) but they are in fact unstable.

In the present analysis, five system parameters (or combinations thereof) control the convection pattern. These parameters are the Stefan number S, the compositional ratio $\mathscr{C}$, the mushy-layer thickness δ, and the permeability coefficients K_1 and K_2. Three parameters, S, $\mathscr{C}$ and δ, control the presence of the oscillatory instability. A simple representation of the regions in parameter space where stable up or down hexagons are possible and where the oscillatory mode is present is shown in figure 3. The shaded region shows where the weakly nonlinear analysis of the steady mode breaks down owing to the interaction of the oscillatory mode (i.e. $a \leqslant 0$ in equation (3.16*a*)). For simplicity we show the leading-order result which corresponds to a curve defined by

$$\frac{2S}{\delta(\mathscr{C}+S)^2} = 1 \tag{4.2}$$

(as can be deduced from equation (3.16*a*)). Outside the shaded region are indicated the regions where stable up or down hexagons are predicted. Here K_1/δ is fixed and for simplicity we have taken $K_2 = 0$. The solid curve (with $K_1/\delta = 0.1$) separates these two domains and corresponds to the parameter values at which the bifurcation to hexagons is vertical ($\epsilon b = 0$, see equation (4.1)). This boundary is given by

$$\frac{3\pi^2}{2}\frac{K_1}{\delta^2\mathscr{C}} = -\frac{4}{3}\left(1+\frac{S}{\mathscr{C}}\right)^2 + \frac{26}{7}\frac{S}{\delta\mathscr{C}^2}. \tag{4.3}$$

The separating curve moves to the left (right) when K_1/δ increases (decreases). The dashed curve indicates the outermost position that this separating curve can attain (corresponding to $K_1/\delta = 0$). Consequently, outside the dashed curve the only stable hexagons are up hexagons. The region between the dashed curve and the boundary of the shaded region is given to leading order by

$$\frac{2S}{\delta\mathscr{C}^2} < \left(1+\frac{S}{\mathscr{C}}\right)^2 < \frac{39}{14}\frac{S}{\delta\mathscr{C}^2}. \tag{4.4}$$

It is interesting to note that the existence of an oscillatory instability and the possibility of stable down hexagons are associated with similar regions in parameter space. In fact, they are both due to the parameter combination $S/\delta\mathscr{C}^2$. Neither of these effects would have been identified had we chosen $S = O(1)$ rather than the distinguished limit $S/\mathscr{C} = O(1)$. We also must note that the region in which down

(a)

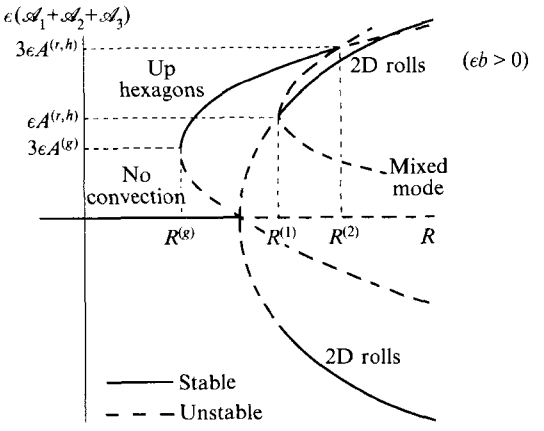

(b)

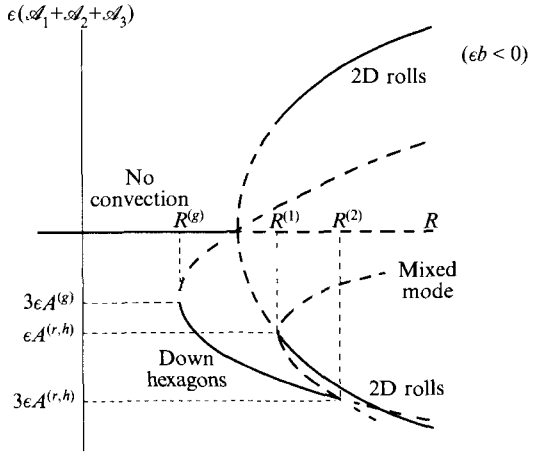

FIGURE 2. Bifurcation diagram. A representation for the amplitude of the nonlinear perturbations $\epsilon(\mathscr{A}_1 + \mathscr{A}_2 + \mathscr{A}_3)$ is plotted *vs.* Rayleigh number for two cases. Solid lines correspond to linearly stable branches while dashed lines represent linearly unstable branches. (*a*) The bifurcation diagram showing the case when $\epsilon b > 0$ (see equation (4.1)). The two-dimensional roll branch bifurcates supercritically and is initially unstable to a subcritically bifurcating hexagonal branch. The stable portion of the hexagonal branch corresponds to hexagons with upflow at the centres (up hexagons). The portion of the branch with $\epsilon(\mathscr{A}_1+\mathscr{A}_2+\mathscr{A}_3) < 0$ corresponds to hexagons with downflow at the centres and is unstable. A mixed mode connects the hexagonal branch to the roll branch at the points where their respective stability changes. This mixed mode is always unstable. (*b*) The bifurcation diagram showing the case when $\epsilon b < 0$ (see equation (4.1)). As in (*a*), the two-dimensional roll branch bifurcates supercritically and is initially unstable to hexagons. The roll and hexagonal branches are again connected via an unstable mixed mode. However, now the stable portion of the hexagonal branch corresponds to hexagons with downflow at the centres (down hexagons). In both (*a*) and (*b*) the limit point of the subcritical hexagon branch corresponds to a Rayleigh number $R^{(g)}$ and amplitude $\epsilon\mathscr{A}_1 = \epsilon\mathscr{A}_2 = \epsilon\mathscr{A}_3 = \epsilon A^{(g)}$. These values represent the global stability limit of the system. We also identify the Rayleigh number at which the two-dimensional roll solution stabilizes and the Rayleigh number at which the hexagonal branch destabilizes as $R^{(1)}$ and $R^{(2)}$, respectively, and note that each is related to the amplitude $\epsilon A^{(r,h)}$.

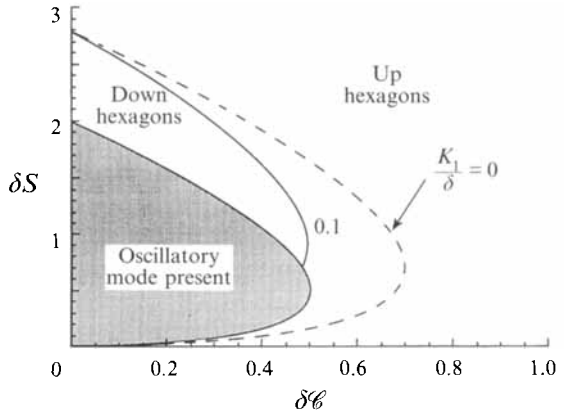

FIGURE 3. Parameter regimes. We identify regions in parameter space δS *vs.* $\delta\mathscr{C}$, for fixed $K_1/\delta = 0.1$ and $K_2 = 0$, where various features of convection in the mushy layer can be identified. The shaded portion corresponds to those parameter values where our weakly nonlinear analysis breaks down owing to the interaction of an oscillatory instability with the steady convective mode. Outside this boundary, we can identify the parameter values for which stable down hexagons or stable up hexagons are predicted. The solid curve (corresponding here to $K_1/\delta = 0.1$) separates the regions where down and up hexagons are predicted. This solid curve moves to the left (right) when K_1/δ increases (decreases). The dashed curve indicates the outermost position that this separating curve can attain (corresponding to $K_1/\delta = 0$). As a result, only up hexagons are possible for parameter values outside the dashed boundary.

hexagons are possible is a somewhat restricted domain. The results in figure 3 show the case where $K_2 = 0$. We find that stable down hexagons cannot be obtained when $K_2 > 0.131$. For values of K_2 larger than this value the right-hand side of equation (4.1) is always positive.

Typical experiments with ammonium chloride, such as those of Tait *et al.* (1992) have $S \approx 5$, $\mathscr{C} \approx 20$ and $\delta \approx 1$. The results shown in figure 3 would therefore suggest that up hexagons should be observed in such experiments. However, it must be remembered that the experiments are conducted with a fixed cooled base rather than at constant growth rate and that the mushy layer is not isolated from the overlying liquid region. Also, the sign of ϵb is quite sensitive to the particular values of the numerical constants multiplying each term. This suggests that while the inclusion of various physical effects in the mushy-layer model is important in explaining the experimentally observed down hexagons, the quantitative predictions in terms of the direction of the flow for hexagonal convection based on these effects could change if a more detailed mushy-layer model were used. In addition, a more detailed model of the mushy layer may introduce further physical effects such as the inclusion of an inflow/outflow upper boundary and these may contribute significantly to the convection pattern predicted. The quantitative results of the present work are therefore not directly applicable to the experimental situation. However, the parametric trends revealed here should be robust and can be used to guide further numerical and experimental investigations.

The bifurcation diagrams in figure 2 show that the points at which two-dimensional rolls and hexagons change their stability are connected in phase space via an unstable mixed mode. The value of the three amplitudes $\epsilon\mathscr{A}_1 = \epsilon\mathscr{A}_2 = \epsilon\mathscr{A}_3 = \epsilon A^{(r,h)}$ associated with the point at which hexagons lose stability is the same amplitude $\epsilon\mathscr{A}_1 = A^{(r,h)}$ at which the two-dimensional rolls stabilize. This has recently been pointed out by

Karcher & Müller (1995) who considered convection in a porous layer where one of the boundaries was a solidification front. As in their work, we can identify the amplitude $\epsilon A^{(r,h)}$ as an alternative pattern selection criterion that can be interpreted as a critical value of the heat transfer induced by convection. That is, for example, if one defines a measure of the heat transfer induced by roll or hexagonal convection as $H = |((\partial\hat{\theta}/\partial z)_{z=0})^2|$ where $||$ represents an appropriate integration over a horizontal area, then $H \sim (\epsilon A)^2$. Corresponding to the amplitude $\epsilon A^{(r,h)}$, one can then identify a critical value of H at which the transition from hexagons to two-dimensional rolls occurs. The Rayleigh numbers and amplitude corresponding to these points in figure 2, which are obtained by analysing the structure and stability of the hexagonal and roll solutions of (3.15) and using equations (3.1*d*), (3.2*f*), (3.8) and (3.16*e*), are given by

$$R^{(1)} = \Omega^{-1/2}\left\{\left[2\pi + \left(\frac{4}{\pi} + \frac{\pi}{2}\right)\frac{S}{\mathscr{C}^2\Omega}\right] + \frac{(\epsilon b)^2 c}{2\pi(d-c)^2}\right\}, \tag{4.5a}$$

$$R^{(2)} = \Omega^{-1/2}\left\{\left[2\pi + \left(\frac{4}{\pi} + \frac{\pi}{2}\right)\frac{S}{\mathscr{C}^2\Omega}\right] + \frac{(\epsilon b)^2(d+2c)}{2\pi(d-c)^2}\right\}, \tag{4.5b}$$

$$\epsilon A^{(r,h)} = \frac{\epsilon b}{d-c}. \tag{4.5c}$$

It is worth pointing out here that the quantity $d - c$ is always positive.

4.2. *Global stability*

We have noted that the bifurcation to hexagonal convection is subcritical with a turning point, or global stability limit, at a value of $R = R^{(g)}$ (see figure 2) that is less than the linear critical point R_{linear}. As is the case whenever a subcritical instability is present, it is of interest to identify how this new global stability limit compares with the linear stability predictions and how it varies with the system control parameters. By the nature of our weakly nonlinear analysis in which amplitudes are assumed to be small, we cannot expect radical variations in the new global stability limit from the linear predictions. Nonetheless, the identification of new stability limits will be of particular interest experimentally and may provide more complete information on ways to avoid convective instabilities altogether in mushy-layer solidification.

An analytical expression for the minimum of the Rayleigh number at which subcritical convective states first appear can be obtained directly from the hexagonal solution to the amplitude equations (3.15) and from equations (3.1*d*), (3.2*f*), (3.8) and (3.16*e*). We express this global stability limit point in terms of original, unscaled, variables and find that

$$R^{(g)} = \Omega^{-1/2}\left\{\left[2\pi + \left(\frac{4}{\pi} + \frac{\pi}{2}\right)\frac{S}{\mathscr{C}^2\Omega}\right] - \frac{9\pi^5}{2\Omega^2}\frac{\left(K_1/\delta\mathscr{C} - K_c/\mathscr{C}\right)^2}{\left[2158\pi^4/259 + 110\pi^4 K_2/\delta^2\Omega^2\mathscr{C}^2 + \delta(c_1 + 2d_1)\right]}\right\}, \tag{4.6}$$

where K_c is as defined in equation (3.13) with $C_S = \delta\mathscr{C}$ and $\bar{S} = \delta S$ and $\Omega = 1 + S/\mathscr{C}$.

Figure 4 shows how this global stability limit $R^{(g)}$ varies as the system parameters S, $\mathscr{C}$, δ and K_1 vary and also compares it with the linear stability predictions R_{linear} of this model. Here we have taken $K_2 = 0$. In figure 4(*a*) the Stefan number is varied while the compositional ratio $\mathscr{C}$, the mushy layer thickness δ and the linear measure of permeability variations K_1 are fixed. Here we see that the trend in the global

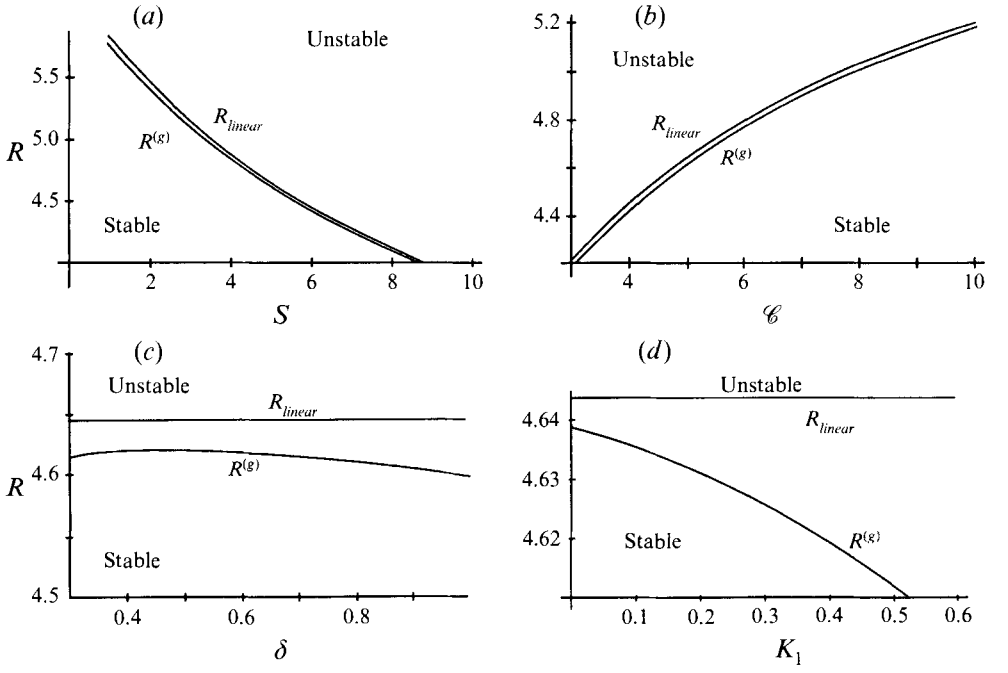

FIGURE 4. Global stability. The global stability limit is compared with the linear critical point as the parameters are varied. In each case $K_2 = 0$ and one parameter is varied while the others are fixed. The parameter ranges shown correspond to the up hexagon branch. (*a*) $K_1 = 0.4$, $\delta = 0.5$ and $\mathscr{C} = 5$ while the Stefan number S is varied. (*b*) $K_1 = 0.4$, $\delta = 0.5$ and $S = 5$ while the compositional ratio $\mathscr{C}$ is varied. (*c*) $K_1 = 0.4$, $\mathscr{C} = 5$ and $S = 5$ while the mushy-layer thickness δ is varied. (*d*) $\delta = 0.5$, $\mathscr{C} = 5$ and $S = 5$ while K_1 is varied.

stability limit $R^{(g)}$ as S varies is dominated by the linear trend so that the system destabilizes when S increases. The explanation for this, as described by Worster (1992*b*), is that as S increases, fluid parcels perturbed upwards can dissolve less and less of the crystals for the same perturbation and therefore cannot take on as much heavy solute.

Figure 4(*b*) shows the variation of $R^{(g)}$ with the compositional ratio $\mathscr{C}$ and also indicates that the trend is dominated by the linear result. However, we see that increasing $\mathscr{C}$ represents a stabilizing effect. In the present analysis $\mathscr{C}$ appears in combination with a number of other parameters. In terms of its effect on the Rayleigh number it appears most strongly in the combination $S/\mathscr{C}$ (hidden in $\Omega^{-1/2}$ in equation (4.6)). So increasing $\mathscr{C}$ has a similar effect to decreasing S. In Worster's (1992*b*) linear stability analysis increasing $\mathscr{C}$ led more strongly to a decrease in porosity and therefore was destabilizing. These two effects can be identified side-by-side if we reconsider the results of Amberg & Homsy (1993) where the leading-order and first correction term to the linear critical Rayleigh number was

$$R = 2\pi + \frac{\pi(K_1 - 2St)}{2\mathscr{C}}, \tag{4.7}$$

according to their equation (3.6) or (3.10) where St is their original Stefan number taken to be $O(1)$. By this result, we can clearly see that the effect of variations in $\mathscr{C}$ depends on the relative strength of K_1 and S. In our analysis we have identified the effect due to the association of $\mathscr{C}$ with S since we have taken S to be large ($O(1/\delta)$) and K_1 to be small ($O(\delta)$).

Figure 4(*c*) shows the effect of varying the thickness of the mushy layer δ. We first note that the effect of δ on the linear critical point does not appear until $O(\delta^2)$ (Amberg & Homsy) so the linear critical Rayleigh number is constant to $O(\delta)$ as δ varies. Also note that the Rayleigh number is based on mushy-layer thickness. We now see that the nonlinear trend due to δ can differ from the linear trend. Here the effect of δ is to amplify the various physical effects associated with the subcritically bifurcating hexagons. The decrease in R on the left side of the plot is associated with increased permeability variations while that on the right is associated with increased curvature of the basic-state temperature profile.

Figure 4(*d*) shows the variation of $R^{(g)}$ with K_1. We see that increasing K_1 destabilizes the system, corresponding to the hexagonal branch becoming more subcritical.

The above results for global stability all correspond to parameter values where only the up hexagon branch is stable (i.e. figure 2*a*). In figure 3 this corresponds to parameter values outside the dashed curve. We can also consider the variation of $R^{(g)}$ across parameter ranges in which the transition from the down hexagon region to the up hexagon region occurs. Since the difference between the linear critical point and the subcritical turning point $R^{(g)}$ is small in these cases, we plot $R^{(g)} - R_{linear}$. Typical results are shown in figure 5. In each plot we can identify the point where vertical bifurcation of the hexagonal branch occurs. This is the point where $R^{(g)} - R_{linear} = 0$. In each case, to the left of this point down hexagons are stable and to the right of this point up hexagons are stable.

Recall that Amberg & Homsy showed that the two-dimensional roll branch can be subcritical for parameter values not considered in the present analysis. We have avoided this possibility by considering only $K_1/\delta\mathscr{C} < 0.226$ but note that such a subcritical instability (present when $K_1/\delta\mathscr{C} > 0.226$) may also affect global stability.

On physical grounds, the perturbation cannot be such that the solid fraction becomes negative. For a given value of δ we expect that there will be some amplitude for which the solid-fraction perturbation is too large. By comparing the basic-state solid-fraction with the solid-fraction perturbation, as was done by Amberg & Homsy (1993), we can identify the perturbation amplitude beyond which negative solid fraction is predicted. These are

$$(\epsilon A)_{max} = \frac{\delta}{12\pi} + O(\delta^2) \qquad \text{for hexagons,} \tag{4.8a}$$

$$(\epsilon A)_{max} = \frac{\delta}{4\pi} + O(\delta^2) \qquad \text{for 2D rolls.} \tag{4.8b}$$

We compare the maximum amplitude for hexagons given in equation (4.8*a*) with the amplitude $\epsilon\mathscr{A}_1 = \epsilon\mathscr{A}_2 = \epsilon\mathscr{A}_3 = \epsilon A^{(g)}$ corresponding to the turning point along the hexagon branch,

$$\epsilon A^{(g)} = \frac{\epsilon b}{2(c + 2d)}, \tag{4.9}$$

as indicated in figure 2, and find that either can be greater. That is, the amplitude at which the model predicts zero solid fraction can occur above the turning point, so steady convection can exist in the mushy layer without the formation of chimneys, or below the turning point, so no steady small-amplitude convection exists before the model breaks down. Similar results hold true if we compare the maximum amplitude for two-dimensional rolls in equation (4.8*b*) with the amplitude $\epsilon A^{(r,h)}$ given by equation (4.5*c*) at which the two-dimensional roll branch becomes stable.

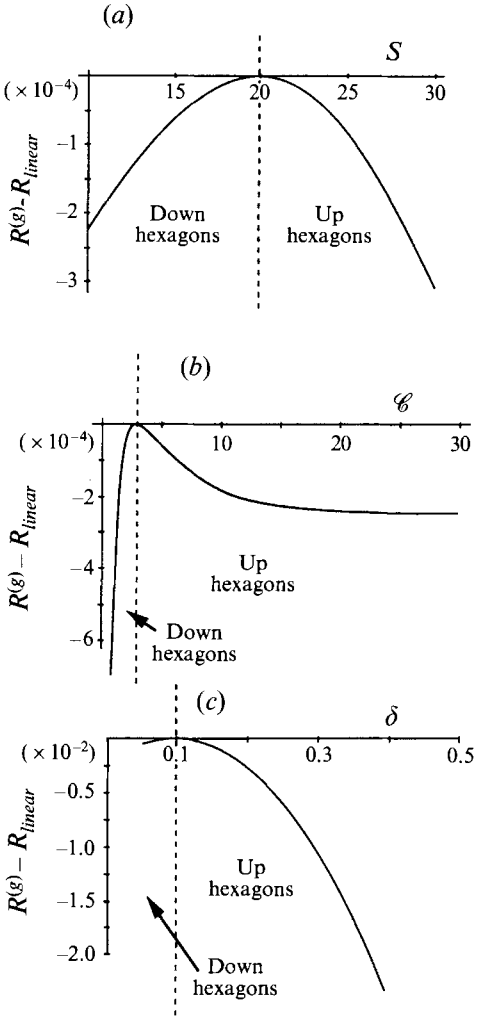

FIGURE 5. Global stability. The difference between the global stability limit and the linear critical point $R^{(g)} - R_{linear}$ is shown. In each case $K_2 = 0$ and $K_1 = 0.01$ and one parameter is varied while the others are fixed. (*a*) $\mathscr{C} = 3$ and $\delta = 0.1$ while the Stefan number S is varied. As S increases, the hexagon branch shifts from that with stable down hexagons to that with stable up hexagons. (*b*) $S = 20$ and $\delta = 0.1$ while the compositional ratio $\mathscr{C}$ is varied. As $\mathscr{C}$ increases, the hexagon branch shifts from that with stable down hexagons to that with stable up hexagons. (*c*) $\mathscr{C} = 3$ and $S = 20$ while the mushy-layer thickness δ is varied. As δ increases, the hexagon branch shifts from that with stable down hexagons to that with stable up hexagons. Notice that as S, $\mathscr{C}$ and δ get small in (*a*), (*b*) and (*c*), respectively, the region where the oscillatory instability interacts is approached.

5. Conclusion

We have considered the stability of nonlinear convecting states in a mushy layer during the solidification of binary alloys. Our analysis is based on a simple model of the mushy layer given by Amberg & Homsy (1993) in which the dynamics of the mushy layer are decoupled from the dynamics of the overlying fluid layer. We performed a weakly nonlinear stability analysis that extends that of Amberg & Homsy (1993) by identifying the stability of steady two-dimensional roll and hexagonal convection patterns, including the relative stability between the two patterns. Of

particular interest and importance in our analysis are the interactions between heat transfer, convection and solidification in the mushy layer. We have found that the inclusion of such interactions leads to the identification of a number of new results.

The pivotal result of our weakly nonlinear analysis is a set of coupled amplitude equations which describe the evolution and stability of small-but-finite-amplitude convecting states in a mushy layer. Analysis of these equations reveals a variety of results regarding convection in the mushy layer.

We have found that the coefficient of the time derivative in the amplitude equations (3.15) can vanish, suggesting the presence of a Hopf bifurcation. We have subsequently analysed the linear stability results in more detail, and have indeed identified an oscillatory instability. The results of our findings are presented in another paper (Anderson & Worster 1995). For the purposes of the present paper, we have simply identified regions where the oscillatory instability does not interact with the steady mode of convection at onset and have focused our attention there.

Our analysis of the steady bifurcating branch shows that either two-dimensional roll or hexagonal convection patterns can be stable. Furthermore, either hexagons with upflow at the centres (up hexagons) or hexagons with downflow at the centres (down hexagons) can be stable. We find that the prediction of the type of hexagons hinges upon the net effect of a variety of physical effects in the mushy layer. Amberg & Homsy identified a single physical effect associated with hexagonal convection, namely that due to nonlinear permeability variations associated with perturbations to the basic-state solid fraction. Based on this effect alone, the theory predicts stable up hexagons but unstable down hexagons. This is in contrast to the experimental results of Tait *et al.* (1992) which showed that down hexagons are observed. The additional physical effects included here correspond to curvature in the temperature profile associated with a uniformly translating mushy layer, higher-order nonuniformities in the permeability due to the basic-state solid fraction and its perturbations, and finally a term representing the nonlinear interactions of temperature and solid fraction. It is the nonlinear interaction between temperature and solid fraction which allows for the possibility of stable down hexagons.

We have also identified new global stability limits associated with the subcritically bifurcating hexagonal solution. We have compared this nonlinear stability limit with the linear stability predictions as the various system control parameters were varied (see figures 4 and 5). The nature of this subcritical stability limit can be such that it represents an approximately uniform shift downwards (destabilizing) in the critical Rayleigh number compared with the linear stability predictions. However, it is also possible that the trends based on the nonlinear results can differ from the linear trends. Such results should aid experimentalists and those in industry in avoiding convective instabilities and the formation of chimneys and freckles altogether.

We have discovered that, for certain parameter values, steady, finite-amplitude convection can occur within a mushy layer without the formation of chimneys, while for other parameter values there is no steadily convecting state with positive values of solid fraction throughout the mushy layer. In other words, in the latter case the growth of infinitesimal disturbances leads inexorably to the formation of chimneys.

It is important to note that the treatment of more detailed models of the mushy layer may alter the quantitative conclusions of this paper. For example, it may be important to include in the analysis the variation of the basic-state permeability and to allow inflow and outflow through the mush–liquid interface. Also, a more detailed model will alter the precise way in which each of these physical effects combines.

That is, the boundary between up hexagons and down hexagons in a more detailed model may shift relative to the present model and as a result may be enough to change the predicted flow direction of hexagons for a particular set of experimentally fixed control parameters. In addition, typical experiments are conducted with a fixed cooled base rather than at constant growth rate and the mushy layer is not physically isolated from the overlying liquid region. Consequently, *quantitative* comparisons with experiments should not be made. However, the *qualitative* results we have discovered (e.g. parametric trends in terms of pattern selection and global stability) should be robust and can be used to guide further numerical and experimental investigations.

We point out here that we have considered a parameter regime, namely that which has $K_1/\delta\mathscr{C} = O(\delta)$ so that the two-dimensional roll solution bifurcates supercritically. Amberg & Homsy have shown that when $K_1/\delta\mathscr{C} > 0.226$ the two-dimensional roll branch bifurcates subcritically. For these parameter values, this together with a subcritically bifurcating hexagonal branch may have important dynamical consequences in terms of global stability.

Finally, we point out that there are important issues regarding nonlinear structure and dynamics of convection in mushy layers still to be addressed, some of which have been pointed out above. The high complexity of the mushy layer and the inherent strongly nonlinear features such as fully developed chimneys suggest that a numerical approach may be needed to make further progress.

This work was supported by grants from the National Aeronautics and Space Administration through the Microgravity Science and Applications Division and from the Natural Environment Research Council. The authors would like to thank B. J. Spencer, M. R. E. Proctor and S. H. Davis for helpful discussions, and are particularly grateful to M. R. E. P. for recognizing the possibility of the Hopf bifurcation.

Appendix. Coefficients in the evolution equation

The following are the expressions for the terms appearing in the evolution equations (3.15).

$$a_1 = \left(\frac{1}{4} - \frac{6}{\pi^2}\right)\frac{\bar{S}}{C_S^2} + \left(6 - \frac{32}{\pi^2}\right)\frac{\bar{S}}{C_S^3\Omega} + \left(\frac{172}{3\pi^2} - \frac{53}{6} - \frac{28}{9\pi}\frac{\sqrt{3}e^{\sqrt{3}\pi}}{e^{2\sqrt{3}\pi}-1} + \frac{2}{9\pi}\frac{\sqrt{3}(1+e^{2\sqrt{3}\pi})}{e^{2\sqrt{3}\pi}-1}\right)\left(\frac{\bar{S}}{C_S^2\Omega}\right)^2, \tag{A 1a}$$

$$c_1 = \left(-\frac{\pi^4}{2} + \frac{32\pi^2}{9}\right)\Omega + \left(\frac{188\pi^2}{63} + \frac{3\pi^4}{2}\right)\frac{\bar{S}}{C_S^2\Omega} - \left(\frac{1904\pi^2}{189} + \frac{19\pi^4}{2}\right)\frac{K_2}{\Omega C_S^2} + \left(\frac{832\pi^2}{9} + 22\pi^4\right)\left(-\frac{K_2}{\Omega^2 C_S^3} + \frac{3}{2}\frac{K_3}{\Omega^2 C_S^3}\right) + \left(\frac{36728\pi^2}{189} + \frac{311\pi^4}{6} + \frac{88\pi^3}{9}\frac{\sqrt{3}e^{\sqrt{3}\pi}}{e^{2\sqrt{3}\pi}-1} - \frac{20\pi^3}{9}\frac{\sqrt{3}(1+e^{2\sqrt{3}\pi})}{e^{2\sqrt{3}\pi}-1}\right)\frac{K_2\bar{S}}{C_S^4\Omega^3}, \tag{A 1b}$$

$$d_1 = \left(-\frac{205\pi^4}{259} + \frac{2354\pi^2}{333}\right)\Omega + \left(\frac{81899\pi^2}{67081} + \frac{615\pi^4}{259}\right)\frac{\bar{S}}{C_S^2\Omega}$$
$$- \left(\frac{141974\pi^2}{6993} + 19\pi^4\right)\frac{K_2}{\Omega C_S^2} + \left(\frac{1664\pi^2}{9} + 44\pi^4\right)\left(-\frac{K_2}{\Omega^2 C_S^3} + \frac{3}{2}\frac{K_3}{\Omega^2 C_S^3}\right)$$
$$+ \left(\frac{73456\pi^2}{189} + \frac{311\pi^4}{3} + \frac{176\pi^3}{9}\frac{\sqrt{3}e^{\sqrt{3}\pi}}{e^{2\sqrt{3}\pi}-1} - \frac{40\pi^3}{9}\frac{\sqrt{3}(1+e^{2\sqrt{3}\pi})}{e^{2\sqrt{3}\pi}-1}\right)\frac{K_2\bar{S}}{C_S^4\Omega^3}. \quad \text{(A 1}c\text{)}$$

REFERENCES

AMBERG, G. & HOMSY, G. M. 1993 Nonlinear analysis of buoyant convection in binary solidification with application to channel formation. *J. Fluid Mech.* **252**, 79–98.

ANDERSON, D. & WORSTER, M. G. 1995 A new oscillatory instability in the mushy layer during solidification of binary alloys. *J. Fluid Mech.* (submitted).

BENNON, W. D. & INCROPERA, F. P. 1987 A continuum model for momentum, heat and species transport in binary solid–liquid phase change systems—I. Model formulation. *Intl J. Heat Mass Transfer* **30**, 2161–2170.

BRATTKUS, K. & DAVIS, S. H. 1988 Cellular growth near absolute stability. *Phys. Rev.* **B 38**, 11452–11460.

BUSSE, F. H. 1967 The stability of finite amplitude cellular convection and its relation to an extremum principal. *J. Fluid Mech.* **30**, 625–649.

CHEN, C. F. & CHEN, F. 1991 Experimental study of directional solidification of aqueous ammonium chloride solution. *J. Fluid Mech.* **227**, 567–586.

CHEN, F., LU, J. W. & YANG, T. L. 1994 Convective instability in ammonium chloride solution directionally solidified from below. *J. Fluid Mech.* **276**, 163–187.

COPLEY, S. M., GIAMEI, A. F., JOHNSON, S. M. & HORNBECKER, M. F. 1970 The origin of freckles in unidirectionally solidified castings. *Metall. Trans.* **1**, 2193–2204.

DAVIS, S. H., MÜLLER, U. & DIETSCHE, C. 1984 Pattern selection in single-component systems coupling Bénard convection and solidification. *J. Fluid Mech.* **144**, 133–151.

DAVIS, S. H. & SEGEL, L. A. 1968 Effects of surface curvature and property variation on cellular convection. *Phys. Fluids* **11**, 470–476.

EMMS, P. W. & FOWLER, A. C. 1994 Compositional convection in the solidification of binary alloys. *J. Fluid Mech.* **262**, 111–139.

FOWLER, A. C. 1985 The formation of freckles in binary alloys. *IMA J. Appl. Maths* **35**, 159–174.

GOLUBITSKY, M., SWIFT, J. W. & KNOBLOCH, E. 1984 Symmetries and pattern selection in Rayleigh–Bénard convection. *Physica* D **10**, 249–276.

HILLS, R. N., LOPER, D. E. & ROBERTS, P. H. 1983 A thermodynamically consistent model of a mushy zone. *Q. J. Mech. Appl. Maths* **36**, 505–539.

KARCHER, C. & MÜLLER, U. 1995 Convection in a porous medium with solidification. *Fluid Dyn. Res.* **15**, 25–42.

KRISHNAMURTI, R. 1968 Finite amplitude convection with changing mean temperature. Part 1. Theory. *J. Fluid Mech.* **33**, 445–455.

KURZ, W. & FISHER D. J. 1989 *Fundamentals of Solidification.* Trans Tech.

KUSKE, R. & MATKOWSKY, B. J. 1994 On roll, square and hexagonal cellular flames. *Eur. J. Appl. Maths* **5**, 65–93.

PALM, E. 1960 On the tendency towards hexagonal cells in steady convection. *J. Fluid Mech.* **8**, 183–192.

PALM, E., WEBER, J. E. & KVERNVOLD, O. 1972 On steady convection in a porous medium. *J. Fluid Mech.* **54**, 153–161.

ROPPO, M. N., DAVIS, S. H. & ROSENBLAT, S. 1984 Bénard convection with time periodic heating. *Phys. Fluids* **27**, 796–803.

SAMPLE, A. K. & HELLAWELL, A. 1984 The mechanisms of formation and prevention of channel segregation during alloy solidification. *Metall. Trans.* **15A**, 2163–2173.

SARAZIN, J. R. & HELLAWELL, A. 1988 Channel formation in Pb-Sn, Pb-Sb, and Pb-Sn-Sb alloy ingots and comparison with the system NH_4Cl-H_2O. *Metall. Trans.* **19A**, 1861–1871.

SCANLON, J. W. & SEGEL, L. A. 1967 Finite amplitude cellular convection induced by surface tension. *J. Fluid Mech.* **30**, 149–162.

SEGEL, L. A. 1965 The non-linear interaction of a finite number of disturbances to a layer of fluid heated from below. *J. Fluid Mech.* **21**, 359–384.

SEGEL, L. A. 1969 Distant side-walls cause slow amplitude modulation of cellular convection. *J. Fluid Mech.* **38**, 203–224.

TAIT, S., JAHRLING, K. & JAUPART, C. 1992 The planform of compositional convection and chimney formation in a mushy layer. *Nature* **359**, 406–408.

TAIT, S. & JAUPART, C. 1992 Compositional convection in a reactive crystalline mush and melt differentiation. *J. Geophys. Res.* **97**(B5), 6735–6756.

VOLLER, V. R. & BRENT, A. D. 1989 The modelling of heat, mass and solute transport in solidification systems. *Intl J. Heat Mass Transfer* **32**, 1719–1731.

WORSTER, M. G. 1986 Solidification of an alloy from a cooled boundary. *J. Fluid Mech.* **167**, 481–501.

WORSTER, M. G. 1991 Natural convection in a mushy layer. *J. Fluid Mech.* **224**, 335–359.

WORSTER, M. G. 1992*a* The dynamics of mushy layers. In *Interactive Dynamics of Convection and Solidification* (ed. S. H. Davis, H. E. Huppert, U. Müller & M. G. Worster), pp. 113–138. Kluwer.

WORSTER, M. G. 1992*b* Instabilities of the liquid and mushy regions during solidification of alloys. *J. Fluid Mech.* **237**, 649–669.